Dinuclear $[Cu_2(N^N)(P^P)_2][PF_6]_2$ complexes containing bridging 2,3,5,6-tetra(pyridin-2-yl)pyrazine or 2,4,6-tri(pyridin-2-yl)-1,3,5-triazine ligands§

Sarah Keller, Alessandro Prescimone, Edwin C. Constable, Catherine E. Housecroft*

Department of Chemistry, University of Basel, Spitalstrasse 51, CH-4056, Basel, Switzerland.

Email: catherine.housecroft@unibas.ch

§This paper is dedicated to Professor Malcolm L. H. Green on the occasion of his 80th birthday in recognition of his exceptional contributions to inorganic and organometallic chemistries.

Abstract

The dinuclear copper(I) complexes $[Cu_2(\mathbf{1})(POP)_2][PF_6]_2$, $[Cu_2(\mathbf{2})(POP)_2][PF_6]_2$, $[Cu_2(\mathbf{1})(xantphos)_2][PF_6]_2$ and $[Cu_2(\mathbf{2})(xantphos)_2][PF_6]_2$ containing bridging 2,3,5,6-tetra(pyridin-2-yl)pyrazine (**1**) or 2,4,6-tri(pyridin-2-yl)-1,3,5-triazine (**2**) ligands and the P^P ligands bis(2-(diphenylphosphino)phenyl)ether (POP) or 4,5-bis(diphenylphosphino)-9,9-dimethylxanthene (xantphos) are presented. The single crystal structures of $[Cu_2(\mathbf{1})(POP)_2][PF_6]_2$ and $[Cu_2(\mathbf{2})(POP)_2][PF_6]_2$ confirm that both **1** and **2** act as bis(bidentate) ligands, bridging between two copper(I) centres; in $[Cu_2(\mathbf{1})(POP)_2][PF_6]_2$, two pyridine rings are non-coordinating, and in $[Cu_2(\mathbf{2})(POP)_2][PF_6]_2$, there is one non-coordinating pyridine. In solution and on the NMR timescale at 295 K, the four pyridine rings in coordinated **1** are equivalent; similarly, the three pyridine donors in the $[Cu_2(\mathbf{2})(P^P)_2][PF_6]_2$ complexes are equivalent. The dynamic behaviour of $[Cu_2(\mathbf{2})(POP)_2][PF_6]_2$ and $[Cu_2(\mathbf{2})(xantphos)_2][PF_6]_2$ are investigated using variable temperature ^{1}H NMR spectroscopy. The photophysical properties of the complexes are discussed.

Keywords: copper; *N*-heterocyclic ligands; bisphosphanes; heteroleptic complexes; X-ray structure

1. Introduction

In contrast to conventional white-light sources, organic light-emitting diodes (OLEDs) and light-emitting electrochemical cells (LECs) exhibit beneficial energy savings [1]. OLED technology is now well established, but the more recently developed LECs offer a number of advantages, including a simpler device architecture and assembly using solution (not vacuum) processing. The active layer in a LEC is a charged material, either an ionic transition metal complex or a polymer [1]. For the former, cyclometallated iridium(III) complexes are the most popular choices, but commercial uptake of iridium-based LECS and OLEDs is limited by the low abundance of iridium in the Earth's crust [2] ($\approx 3 \times 10^{-6}$ ppm). In contrast, copper is highly abundant and cheap [3], and over the last few years, the potential for copper-containing OLEDs [4] and LECs [5,6,7,8] has come to the fore. Among the most promising emissive copper(I) complexes are heteroleptic $[Cu(P\text{^}P)(N\text{^}N)]^+$ species in which N^N is a diimine ligand and P^P is a sterically demanding bis(phosphino) chelate such as bis(2-(diphenylphosphino)phenyl)ether (POP) or 4,5-bis(diphenylphosphino)-9,9-dimethylxanthene (xantphos) [5,6,8–20]. A number of related dicopper complexes have also been reported [21,22,23,24].

Few studies have focused on dinuclear copper complexes for application in LECs. Brüggler, De Cola and coworkers have described the use of rigid tetra(phosphino) units as the bridging domains in dicopper(I) complexes [25], while the groups of Delavaux, Armaroli and Nierengarten [26] and of Weinhardt, Baumann and Bräse [27] have focused on the use of P^N

bridging domains. As an extension of our studies of $[Cu(N^N)(POP)]^+$ complexes in which the N^N domain is a 2,2':6',2''-terpyridine (tpy) ligand [28], we now report a series of four dinuclear complexes of type $[Cu_2(P^P)_2(\mu\text{-}L)]^{2+}$ in which P^P is either POP or xantphos and μ-L is 2,3,5,6-tetra(pyridin-2-yl)pyrazine (**1**) or 2,4,6-tri(pyridin-2-yl)-1,3,5-triazine (**2**) (Scheme 1).

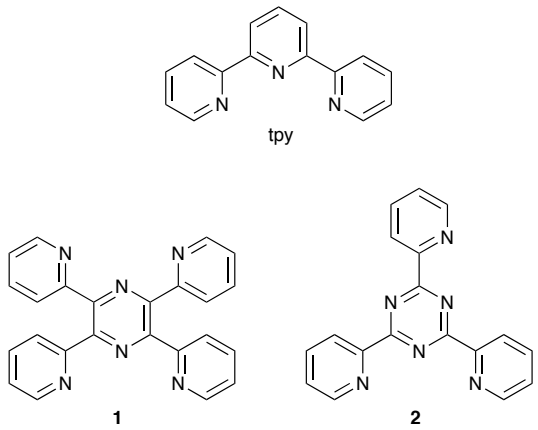

Scheme 1. The structures of ligands **1** and **2**, and a comparison of their metal-binding domains with that of 2,2':6',2''-terpyridine (tpy).

2. Experimental

2.1 General

^1H, ^{13}C and ^{31}P NMR spectra were recorded on Bruker Avance III-600, III-500 or III-400 NMR spectrometers. ^1H and ^{13}C NMR chemical shifts were referenced to residual solvent peaks with respect to δ(TMS) = 0 ppm and ^{31}P NMR chemical shifts with respect to δ(85% aqueous H_3PO_4) = 0 ppm. Solution absorption and emission spectra were recorded with an Agilent 8453 spectrophotometer and Shimadzu RF-5301PC spectrofluorometer, respectively. Electrospray ionization (ESI) mass spectra were recorded on a Bruker esquire 3000plus instrument.

2.2 $[Cu_2(1)(POP)_2][PF_6]_2$

A colourless solution of $[Cu(MeCN)_4][PF_6]$ (112 mg, 0.30 mmol) and POP (162 mg, 0.30 mmol) in CH_2Cl_2 (40 mL) was stirred for 2 h. Then **1** (58 mg, 0.15 mmol) was added and the bright red solution was stirred for another 2 h. The solution was filtered and the filtrate evaporated to dryness. The red residue was redissolved in CH_2Cl_2 (4 mL), transferred to a tube and the solution layered with Et_2O. This yielded red crystalline $[Cu_2(\mathbf{1})(POP)_2][PF_6]_2$ (140 mg, 0.074 mmol, 49%). ^{1}H NMR (500 MHz, CD_2Cl_2, 295 K) δ/ppm 8.24 (d, J = 4.7 Hz, 4H, H^{B6}), 7.28 (t, J = 7.9 Hz, 4H, H^{B4}), 7.24 (overlapping m, 12H, H^{C5+D4}), 7.13–7.06 (m, 20H, H^{D3+B5}), 7.09 (m, 4H, H^{B5}), 6.98 (t, J = 7.5 Hz, 4H, H^{C4}), 6.91 (m, 4H, H^{C6}), 6.86 (m, 16H, H^{D2}), 6.69 (d, J = 7.9 Hz, 4H, H^{B3}), 6.66 (m, 4H, H^{C3}). $^{13}C\{^1H\}$ NMR (126 MHz, CD_2Cl_2, 295 K) δ/ppm 157.6 (C^{C1}), 153.1 ($C^{A2/B2}$), 150.4 ($C^{A2/B2}$), 150.2 (C^{B6}), 138.3 (C^{B4}), 134.9 (C^{C3}), 132.8 (C^{C5}), 131.0 (C^{D4}), 130.5 (C^{D1}), 129.5 (C^{D3}), 127.1 (C^{B3}), 126.5 (C^{B5}), 125.9 (C^{C4}), 120.4 (C^{C6}), C^{C2} not resolved. $^{31}P\{^1H\}$ NMR (202 MHz, CD_2Cl_2). δ/ppm −11.8 (br, FWHM = 130 Hz, POP), −144.7 (septet, J_{PF} = 711 Hz, $[PF_6]^-$). UV-Vis (CH_2Cl_2, 2.5 × 10^{-5} mol dm^{-3}): λ / nm (ε / dm^3 mol^{-1} cm^{-1}) 272sh (50630), 346 (20450), 485 (4480). ESI MS: *m/z* 989.7 $[Cu(\mathbf{1})(POP)]^+$ (base peak, calc. 989.2), 601.4 $[Cu(POP)]^+$ (calc. 601.1). Found C 61.36, H 4.22, N 4.78; $C_{96}H_{72}Cu_2F_{12}N_6O_2P_6$ requires C 61.25, H 3.86, N 4.46%.

2.3 $[Cu_2(2)(POP)_2][PF_6]_2$

A solution of $[Cu(MeCN)_4][PF_6]$ (93 mg, 0.25 mmol) and POP (134 mg, 0.25 mmol) in CH_2Cl_2 (40 mL) was stirred for 2 h. Then **2** (39 mg, 0.125 mmol) was added and the dark red solution was stirred for 2 h. The solution was filtered and the filtrate evaporated to dryness. $[Cu_2(\mathbf{2})(POP)_2][PF_6]_2$ was isolated as a dark red powder (185 mg, 0.102 mmol,

82%). ^{1}H NMR (500 MHz, CD_2Cl_2, 295 K) δ/ppm 8.19 (broad, see text), 7.33 (m, 7H, H^{C5+B5}), 7.25 (t, J = 7.5 H, 8H, H^{D4}), 7.11 (t, J = 7.6 Hz, 4H, H^{C4}), 7.06-6.94 (broad m, 20H, H^{D3+C6}), 6.89 (m, 4H, H^{C3}), 6.78 (m, 16H, H^{D2}). $^{13}C\{^{1}H\}$ NMR (126 MHz, CD_2Cl_2) δ/ppm 158.1 (t, J = 6.0 Hz, C^{C1}), 134.7 (C^{C3}), 133.5 (br, C^{D2}), 133.1 (C^{C5}), 130.9 (C^{D4}), 130.6 (C^{D1}), 130.1 (C^{B5}), 129.4 (t, J = 5.1 Hz, C^{D3}), 126.1 (C^{C4}), 124.5 (t, J = 15.4 Hz, C^{C2}), 120.5 (C^{C6}), $C^{A2,B2,B3,B4}$ not resolved. $^{31}P\{^{1}H\}$ NMR (202 MHz, CD_2Cl_2). δ/ppm −10.9 (br, FWHM = 130 Hz, POP), −144.4 (septet, J_{PF} = 711 Hz, $[PF_6]^-$). UV-Vis (CH_2Cl_2, 2.5 × 10^{-5} mol dm^{-3}): λ / nm (ε / dm^3 mol^{-1} cm^{-1}) 277 (55440), 489 (6340). ESI MS: *m/z* 913.6 $[Cu(\mathbf{2})(POP)]^+$ (base peak, calc. 913.20), 601.4 $[Cu(POP)]^+$ (calc. 601.09). Found C 59.25, H 4.22, N 4.77; $C_{90}H_{68}Cu_2F_{12}N_6O_2P_6$ requires C 59.84, H 3.79, N 4.65%.

2.4 $[Cu_2(\mathbf{1})(xantphos)_2][PF_6]_2$

A solution of $[Cu(MeCN)_4][PF_6]$ (112 mg, 0.30 mmol) and xantphos (174 mg, 0.30 mmol) in CH_2Cl_2 (40 mL) was stirred for 2 h, after which **1** (58 mg, 0.15 mmol) was added. The dark red solution was stirred for 2 h, and then filtered. After removal of solvent from the filtrate, $[Cu_2(\mathbf{1})(xantphos)_2][PF_6]$ was isolated as a red powder (285 mg, 0.15 mmol, 97%). ^{1}H NMR (500 MHz, CD_2Cl_2, 295 K) δ/ppm 7.93 (broad, see text), 7.63 (dd, J = 7.8, 1.2 Hz, 4H, H^{C5}), 7.26 (overlapping m, 12H, H^{D4+C4}), 7.17 (t, J = 7.5 Hz, 16H, H^{D3}), 7.09 (m, 16H, H^{D2}), 6.97 (broad, see text), 6.84 (m, 4H, H^{C3}), 6.72 (broad, see text), 1.61 (s, 12H, $H^{xantphos\text{-}Me}$). $^{13}C\{^{1}H\}$ NMR (126 MHz, CD_2Cl_2) δ/ppm 154.6 (C^{C1}), 153.2 ($C^{A2/B2}$), 152.2 ($C^{A2/B2}$), 150.1 (C^{B6}), 137.4 (br, C^{B4}), 134.2 (C^{C6}), 133.3 (t, J_{PC} = 8.2 Hz, C^{D2}), 131.2 (m, C^{D1}), 130.9 (C^{D4}), 129.5 (t, J_{PC} = 4.8 Hz, C^{D3}), 128.1 (C^{C5}), 126.4 (br, $C^{B3/B5}$), 126.2 (br, $C^{B3/B5}$), 125.6 (C^{C4}), 119.5 (m, C^{C2}), 36.2 ($C^{xantphos\text{-}bridge}$), 28.2 ($C^{xantphos\text{-}Me}$). $^{31}P\{^{1}H\}$ NMR (202 MHz, CD_2Cl_2) δ/ppm −13.8 (FWHM = 45 Hz, xantphos), −144.6 (septet, J_{PF} = 711 Hz, $[PF_6]^-$). UV-

Vis (CH_2Cl_2, 2.5 × 10^{-5} mol dm^{-3}): λ / nm (ε / dm^3 mol^{-1} cm^{-1}) 275 (58180), 333 (18460), 485 (5390). ESI MS: *m/z* 1029.7 [Cu(**1**)(xantphos)]$^+$ (calc. 1029.3), 641.4 [Cu(xantphos)]$^+$ (calc. 641.1), 611.4 [(xantphos)O_2+H]$^+$ (calc. 611.2). Found C 60.22, H 4.11, N 4.28; $C_{102}H_{80}Cu_2F_{12}N_6O_2P_6 \cdot H_2O$ requires C 61.85, H 4.17, N 4.24%.

2.4 $[Cu_2(2)(xantphos)_2][PF_6]_2$

A CH_2Cl_2 (40 mL) solution of $[Cu(MeCN)_4][PF_6]$ (112 mg, 0.30 mmol) and xantphos (174 mg, 0.30 mmol) was stirred for 2 h. Then **2** (47 mg, 0.15 mmol) was added. The red solution was stirred for 2 h, then was filtered and the filtrate evaporated to dryness. $[Cu_2(\mathbf{2})(xantphos)_2][PF_6]_2$ was isolated as a dark red powder (265 mg, 0.140 mmol, 93.6%). ^{1}H NMR (500 MHz, CD_2Cl_2, 295 K) δ/ppm 8.90 (br), 8.83 (br), 8.29 (br), 8.25 (br), 7.70 (d, *J* = 7.7 Hz), 7.65 (dd, *J* = 7.8, 1.4 Hz), 7.41 (br), 7.33–7.21 (br), 7.21 (t, *J* = 7.7 Hz), 7.05 (br), 6.99 (br), 6.87 (br), 6.09 (br), 5.82 (br). ^{13}C{^{1}H} NMR (126 MHz, CD_2Cl_2, 295 K, see text) δ/ppm 155.1 (t, J_{PC} = 6.4 Hz, C^{C1}), 150.0, 140.6, 134.4 (C^{C6}), 133.2 (t, J_{PC} = 7.6 Hz), 131.0, 129.8, 129.3, 128.5 (C^{C5}), 125.8 (C^{C4}), 119.5 (m, C^{C2}), 36.4 ($C^{xantphos\text{-}bridge}$), 31.1 ($C^{xantphos\text{-}Me}$), 26.2 ($C^{xantphos\text{-}Me}$), see text discussion. ^{31}P{^{1}H} NMR (202 MHz, CD_2Cl_2) δ/ppm −12.2 (br, FWHM = 100 Hz, xantphos), −144.4 (septet, J_{PF} = 711 Hz, $[PF_6]^-$). UV-Vis (CH_2Cl_2, 2.5 × 10^{-5} mol dm^{-3}): λ/nm (ε / dm^3 mol^{-1} cm^{-1}) 279 (71920), 486 (6200). ESI MS: *m/z* 953.6 [Cu(**1**)(xantphos)]$^+$ (calc. 953.2), 611.4 [(xantphos)O_2+H]$^+$ (calculated 611.2). Found C 61.02, H 4.42, N 4.77; $C_{96}H_{76}Cu_2F_{12}N_6O_2P_6$ requires C 61.12, H 4.06, N 4.45%.

2.5 Crystallography

Data were collected on a Bruker Kappa Apex2 diffractometer with data reduction, solution and refinement using APEX [29] and CRYSTALS [30]. The program Mercury v.

3.5.1 [31,32] was used to draw ORTEP diagrams and for structural analysis. It was necessary to use SQUEEZE [33] to treat the solvent region of the complex with ligand **2**, and the electron density removed equated to 1.8 molecules of CH_2Cl_2 per two Cu atoms.

2.6 $[Cu_2(1)(POP)_2][PF_6]_2 \cdot 4H_2O$

$C_{96}H_{80}Cu_2F_{12}N_6O_6P_6$, M = 1950.20, red block, triclinic, space group $P\bar{1}$, a = 11.4824(4), b = 12.9997(5), c = 17.5773(7) Å, α = 105.577(2), β = 90.915(3), γ = 90.160(2)°, U = 2526.97(17) Å^3, Z = 1, D_c = 1.281 Mg m^{-3}, μ(Cu-Kα) = 2.047 mm^{-1}, T = 123 K. Total 37988 reflections, 9357 unique, R_{int} = 0.061. Refinement of 7405 reflections (571 parameters) with $I > 2\sigma(I)$ converged at final R_1 = 0.0914 (R_1 all data = 0.1094), wR_2 = 0.2375 (wR_2 all data = 0.2493), gof = 0.9582.

2.7 $[Cu_2(2)(POP)_2][PF_6]_2 \cdot 1.8CH_2Cl_2$

$C_{91.8}H_{71.6}Cu_2F_{12}N_6O_2P_6Cl_{3.6}$, M = 1958.11, red block, triclinic, space group $P\bar{1}$, a = 13.5571(8), b = 17.2958(10), c = 20.1831(11) Å, α = 103.019(3), β = 90.392(3), γ = 104.416(3)°, U = 4455.8(2) Å^3, Z = 2, D_c = 1.46 Mg m^{-3}, μ(Cu-Kα) = 3.232 mm^{-1}, T = 123 K. Total 47969 reflections, 15698 unique, R_{int} = 0.039. Refinement of 12059 reflections (1099 parameters) with $I > 2\sigma(I)$ converged at final R_1 = 0.0470 (R_1 all data = 0.0620), wR_2 = 0.1207 (wR_2 all data = 0.1372), gof = 0.91890.

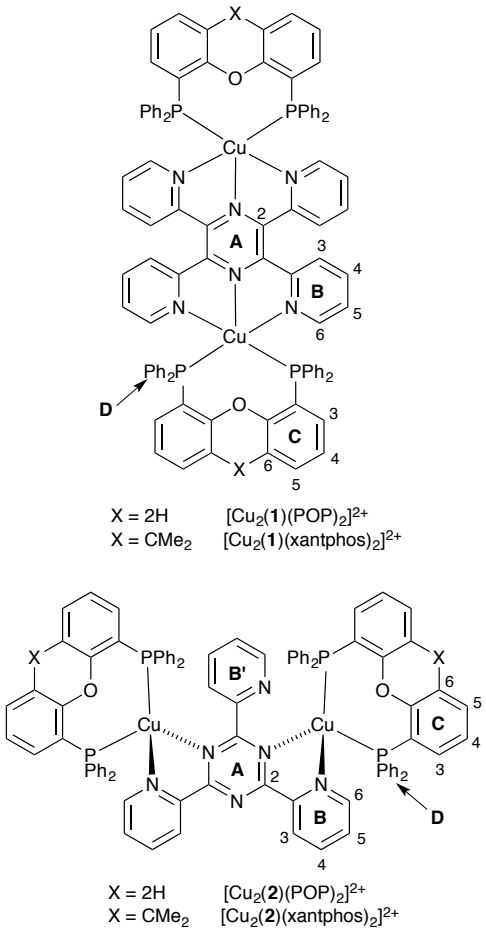

Scheme 2. Structures of complexes with atom labelling for NMR spectroscopic characterization.

3 Results and discussion

3.1 Synthesis and structural characterization of complexes

The copper complexes (Scheme 2) were prepared by first [5] combining $[Cu(MeCN)_4][PF_6]$ with POP or xantphos, followed by the addition of **1** or **2**. The products were obtained as red solids in yields ranging from 49 to 97%. The highest mass peak envelope in the electrospray mass spectrum of each complex corresponded to $[Cu(P\text{^}P)(\mathbf{1})]^+$ or $[Cu(P\text{^}P)(\mathbf{2})]^+$; no molecular ion corresponding to a dicopper species was detected.

Satisfactory elemental analyses were obtained for the complexes, but to confirm the dinuclear nature of the complexes, single crystal structure data were necessary.

The crystal structures of $[Cu_2(\mathbf{1})(POP)_2][PF_6]_2 \cdot 2H_2O$ and $[Cu_2(\mathbf{2})(POP)_2][PF_6]_2 \cdot 1.8CH_2Cl_2$ were determined. For the latter, the program SQUEEZE [33] was used to treat the solvent region, and the electron density removed equated to 1.8 molecules of CH_2Cl_2 per two Cu atoms. Both compounds crystallize in the centrosymmetric space group *P*–1, and in $[Cu_2(\mathbf{1})(POP)_2][PF_6]_2 \cdot 4H_2O$, the $[Cu_2(\mathbf{1})(POP)_2]^{2+}$ cation resides on an inversion centre (Fig. 1). Ligand **1** binds in a bis(bidentate) mode, with Cu–N bonds lengths of 2.146(4) and 2.075(4) Å (see caption to Fig. 1) and a long non-bonded separation for the third donor (Cu1...N3 = 3.165(5) Å). Atom Cu1 is in a distorted tetrahedral environment with angles ranging from 79.47(15) to 134.21(11)^o (see Fig. 1 caption). The Cu–P bond distances and P1–Cu1–P2 angle are as expected (see caption to Fig. 1). The coordinated pyridylpyrazine unit is significantly twisted (angle between the ring planes = 34.9^o), and for each ring, the Cu–N vector deviates substantially from the plane of the heterocycle. We [6] and others [34] have previously commented upon this phenomenon in $[M(POP)(N\text{^}N)]^+$ complexes with M = Cu or Ag. The ring containing N3 is twisted 64.2^o with respect to the plane of the coordinated pyridine ring containing N2, and engages in a face-to-face π-stacking interaction with the pyrazine ring. A second interaction generated by inversion leads to the triple-decker stack shown in Fig. 2; this is characterized by centroid...centroid and centroid...plane separations of 3.77 and 3.65 Å, respectively, and an interplane angle of 11.4^o (which is non-optimal for the π-contact).

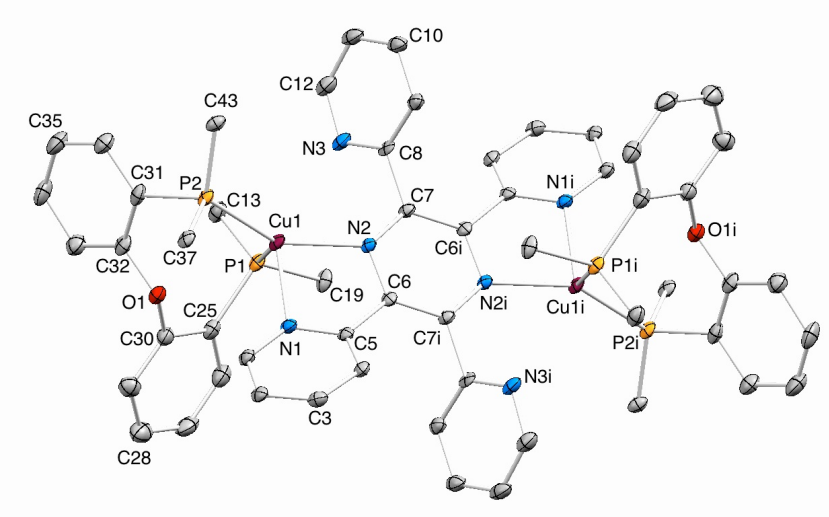

Fig. 1. Structure of the $[Cu_2(\mathbf{1})(POP)_2]^{2+}$ cation in $[Cu_2(\mathbf{1})(POP)_2][PF_6]_2{\cdot}4H_2O$; H atoms are omitted for clarity, and only the *ipso*-C atoms of the phenyl rings are shown. Ellipsoids are plotted at 40% probability level. Symmetry code i = –*x*, 2–*y*, –*z*. Selected bond parameters: Cu1–P1 = 2.2693(14), Cu1–P2 = 2.2328(13), Cu1–N1 = 2.146(4), Cu1–N2 = 2.075(4) Å; P1–Cu1–P2 = 117.05(5), P1–Cu1–N1 = 106.65(12), P2–Cu1–N1 = 104.32(11), P1–Cu1–N2 = 104.67(11), P2–Cu1–N2 = 134.21(11), N1–Cu1–N2 = 79.47(15)°. Colour online.

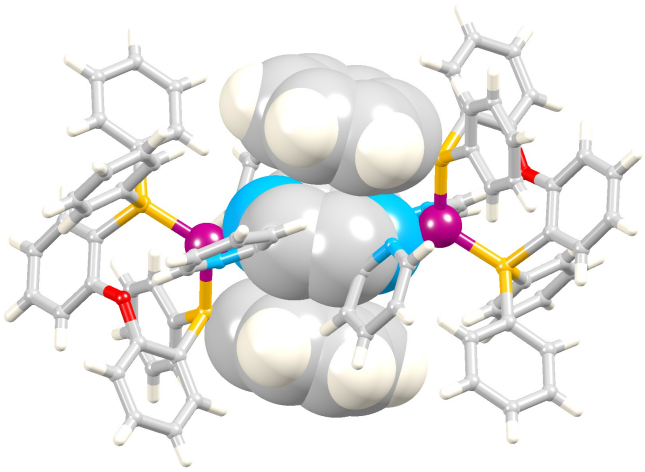

Fig. 2. Centrosymmetric triple decker π-stack in the $[Cu_2(\mathbf{1})(POP)_2]^{2+}$ cation. Colour online.

Fig. 3 shows the structure of the $[Cu_2(\mathbf{2})(POP)_2]^{2+}$ cation in $[Cu_2(\mathbf{2})(POP)_2][PF_6]_2{\cdot}1.8CH_2Cl_2$. The bis(bidentate) coordination mode of ligand **2** leaves atom N6 of the triazine ring and one pyridine ring uncoordinated. Each Cu atom has a distorted tetrahedral geometry with a range of angles of 79.32(10) to 132.90(7)° for Cu1, and 79.17(10) to 128.80(8)° for Cu2; bond distances are unexceptional (see caption to

Fig. 2). Although the *O*-donors in the POP ligand are not bound to copper, one Cu...O distance is rather short (Cu2...O2 = 2.825(2) Å, compared to Cu1...O1 = 3.034(2) Å). These values straddle the one in the $[Cu_2(\mathbf{1})(POP)_2]^{2+}$ cation (Cu1...O1 = 2.966(4) Å.

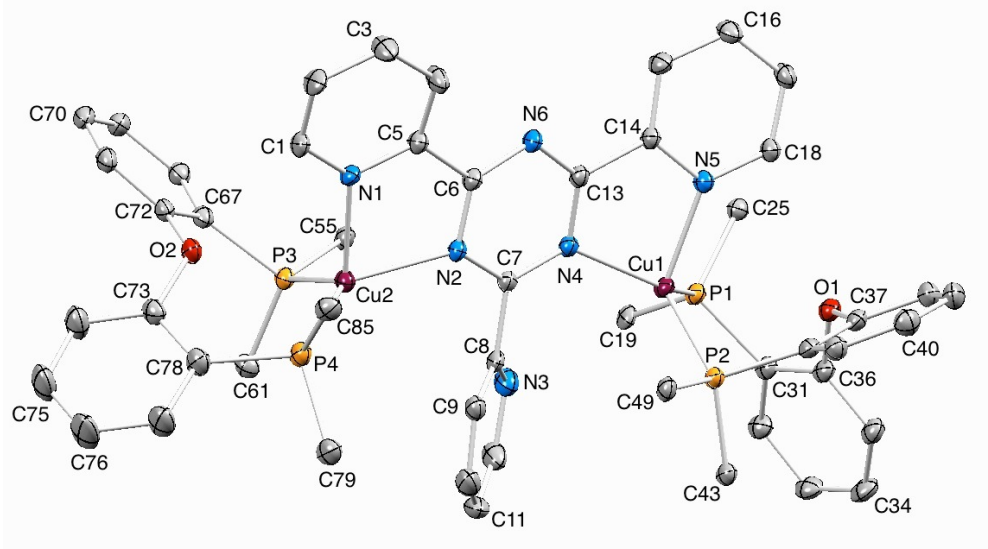

Fig. 3. Structure of the $[Cu_2(\mathbf{2})(POP)_2]^{2+}$ cation in $[Cu_2(\mathbf{2})(POP)_2][PF_6]_2 \cdot 1.8CH_2Cl_2$; for clarity, H atoms are omitted and only the *ipso*-C atoms of the phenyl rings are shown. Ellipsoids are plotted at 40% probability level. Selected bond parameters: Cu1–P1 = 2.2563(9), Cu1–P2 = 2.2677(9), Cu1–N4 = 2.115(2), Cu1–N5 = 2.115(3), Cu2–P3 = 2.2302(9), Cu2–P4 = 2.2381(9), Cu2–N1 = 2.116(3), Cu2–N2 = 2.114(3) Å; P1–Cu1–P2 = 115.07(3), P1–Cu1–N4 = 132.90(7), P2–Cu1–N4 = 106.87(7), P1–Cu1–N5 = 104.88(7), P2–Cu1–N5 = 109.32(8), N4–Cu1–N5 = 79.32(10), P3–Cu2– P4 = 118.57(4), P3–Cu2–N1 = 113.27(8), P4–Cu2–N1 = 102.17(8), P3–Cu2–N2 = 106.65(8), P4–Cu2–N2 = 128.80(8), N1–Cu2–N2 = 79.17(10)°. Colour online.

The non-coordinated pyridyl ring in the $[Cu_2(\mathbf{2})(POP)_2]^{2+}$ cation is hosted within a cavity between four phenyl rings, one from each PPh_2 unit (Fig. 4a); however, only one edge-to-face π-contact is efficient (CH...centroid = 2.55 Å). Despite the multiple arene rings in the $[Cu_2(\mathbf{2})(POP)_2]^{2+}$ cation, only two face-to-face π-stacking interactions occur (Fig. 4b), and neither has optimal metric characteristics. The first π-contact is within one POP ligand (angle between ring planes = 14.3°, centroid...ring plane = 3.62 Å, distance between ring centroids = 3.74 Å) and the second is between the phenyl ring with C85

and the pyridine ring of **2** containing N1 (angle between ring planes = 21.6°, centroid...ring plane = 3.41 Å, centroid...centroid separation = 3.77 Å).

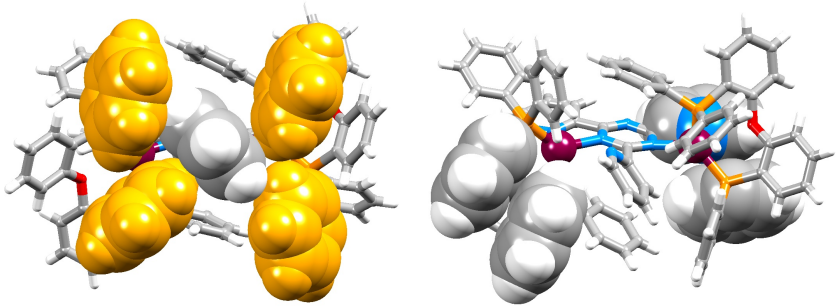

(a) (b)

Fig. 4. The $[Cu_2(\mathbf{2})(POP)_2]^{2+}$ cation showing (a) accommodation of the non-coordinated pyridyl ring within a cavity of four phenyl rings of PPh_2 units, and (b) face-to-face π-stacking interactions within one POP ligand (left) and between POP and ligand **2** (right). Colour online.

Preliminary single crystal data for $[Cu_2(\mathbf{1})(xantphos)_2][PF_6]_2$ were obtained and confirmed that, like $[Cu_2(\mathbf{1})(POP)_2][PF_6]_2 \cdot 4H_2O$, the complex crystallizes in the space group P–1 with centrosymmetric dinuclear $[Cu_2(\mathbf{1})(xantphos)_2]^{2+}$ cations in which ligand **1** is bidentate.

Solution NMR spectroscopic properties

Solution ^1H and ^{13}C NMR spectra of $[Cu_2(\mathbf{1})(POP)_2][PF_6]_2$, $[Cu_2(\mathbf{2})(POP)_2][PF_6]_2$, $[Cu_2(\mathbf{1})(xantphos)_2][PF_6]_2$ and $[Cu_2(\mathbf{2})(xantphos)_2][PF_6]_2$ were recorded in CD_2Cl_2 and were assigned using COSY, NOESY, HMQC and HMBC methods. Ligand **1** presents two tpy metal-binding domains in a 'back-to-back' arrangement. The solid-state structure of $[Cu_2(\mathbf{1})(POP)_2][PF_6]_2$ (Fig. 1) shows **1** acting as a bis(bidentate) ligand, with two uncoordinated pyridine rings. However, in solution at 295 K, the ^1H NMR spectrum of $[Cu_2(\mathbf{1})(POP)_2][PF_6]_2$ (Fig. 5a) exhibits only one set of signals for the four pyridine rings

(ring B, Scheme 2). This is consistent with either **1** functioning as two tpy domains, or a low energy dynamic process interconverting bpy domains as shown in Scheme 3. This mimics what is observed in [Cu(POP)(tpy)][PF_6] and related complexes [28,35]. The close proximity of the two metal-binding sites results in the signal for H^{B3} (which resides above the ring current of a pyridine ring of the adjacent tpy domain) appearing at relatively low frequency (δ 6.69 ppm compared to δ 7.80 ppm in [Cu(POP)(tpy)][PF_6] [28]). A less drastic shift is seen for the signal for H^{B4} (δ 7.28 ppm in [Cu_2(**1**)(POP)$_2$][PF_6]$_2$ versus δ 7.62 ppm in [Cu(POP)(tpy)][PF_6] [28]).

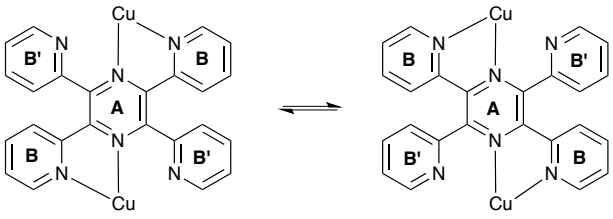

Scheme 3. Interconversion of two bpy metal-binding domains renders rings B and B' equivalent.

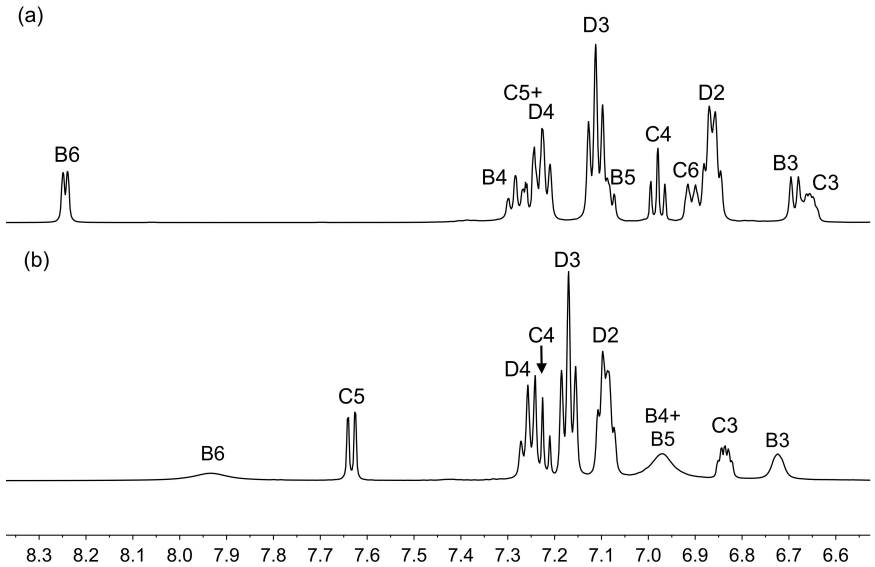

Fig. 5. Aromatic region of the 500 MHz ^{1}H NMR spectra of a CD_2Cl_2 solution at 295 K of (a) [Cu_2(**1**)(POP)$_2$][PF_6]$_2$ and (b) [Cu_2(**1**)(xantphos)$_2$][PF_6]$_2$. Chemical shifts in δ/ppm.

Fig. 5 shows a comparison of the aromatic region of the ^{1}H NMR spectra of $[Cu_2(\mathbf{1})(POP)_2][PF_6]_2$ and $[Cu_2(\mathbf{1})(xantphos)_2][PF_6]_2$. The loss of the signal for H^{C6} on going from Fig. 5a to 5b is consistent with the introduction of the bridging CMe_2 in xantphos. A significant change is the broadening and shifting to lower frequency of the signals for the pyridine ring protons. The signals for H^{B3}, H^{B4}, H^{B5} and H^{B6} (Fig. 5b) were assigned combining the characteristic ^{13}C chemical shifts of C^{B6} and C^{B4} (see the HMQC spectrum in Fig. 6) and the appearance of an H^{B3}/H^{B4} crosspeak in the COSY spectrum. The appearance of the pyridine proton signals at 295 K (Fig. 5b) is most likely associated with dynamic processes involving (i) the interconversion shown in Scheme 3, and (ii) inversion of the bowl-like xanthene unit. We have previously described the interconversion of conformers via xanthene inversion in the related complex $[Cu(Phbpy)(xantphos)][PF_6]$ (Phbpy = 6-phenyl-2,2'-bipyridine) [36] and we return to this below.

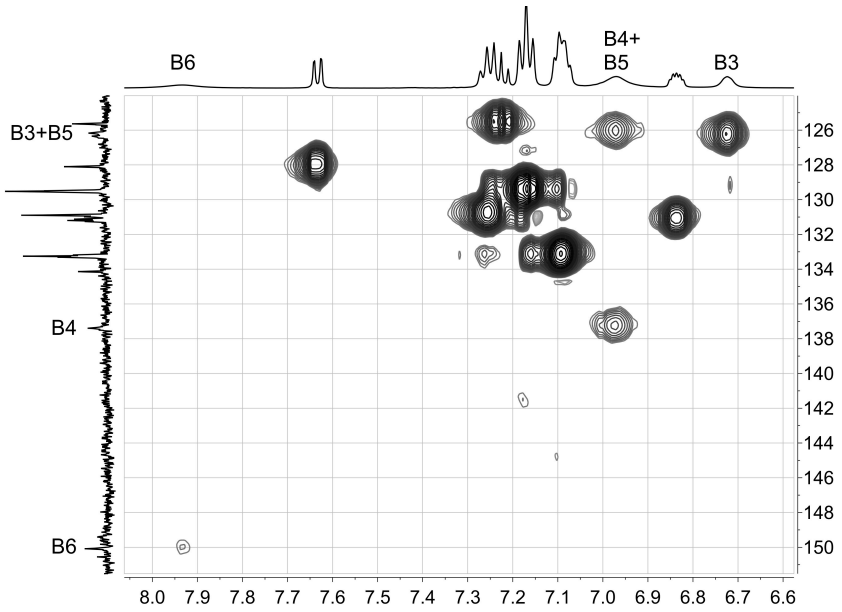

Fig. 6. Part of the HMQC spectrum (applied magnetic field = 11.75 T) of $[Cu_2(\mathbf{1})(xantphos)_2][PF_6]_2$ (in CD_2Cl_2) showing pyridine ring ^{1}H and ^{13}C NMR signal assignments. Chemical shifts in δ/ppm.

At room temperature, the solution ^{1}H NMR spectrum of $[Cu_2(\mathbf{2})(POP)_2][PF_6]_2$ exhibits signals arising from the POP ligand and a broad signal at δ 8.19 ppm (top spectrum in Fig. 7). Use of COSY, HMQC and HMBC allowed the POP ligand resonances to be assigned. In the HMQC spectrum (Fig. 8), the broad ^{1}H NMR signal at δ 8.19 ppm showed a correlation to a ^{13}C resonance at δ 150.1 ppm (unresolved in the 1D spectrum), allowing this to be assigned to H^{B6}; this is analogous to the crosspeak assignment shown in Fig. 5 for $[Cu_2(\mathbf{1})(POP)_2][PF_6]_2$. In addition, the ^{1}H NMR signal at δ 7.32 ppm gave two correlation peaks to δ^{13}C 130.1 ppm (unresolved in the 1D spectrum, Fig. 8) and δ^{13}C 133.1 ppm assigned to C^{B5} and C^{C5}, respectively. Upon cooling (Fig. 7), all signals initially collapse. At 215 K, ligand **2** exhibits two pyridine environments in a ratio of 2 : 1, consistent with two chelating bpy domains and one non-coordinated pyridine ring, as seen in the solid-state structure (Fig. 3). The C ring of the POP ligand retains one environment between 295 and 215 K, while the phenyl rings D separate into two environments (Fig. 7). The observations can be rationalized in terms of two dynamic processes. Cooling the sample first freezes out a process that renders the three pyridine rings equivalent, a process related to that in Scheme 3 but involving only one pendant pyridine ring. As the pyridine rings in ligand **2** separate into the chelating and non-coordinated sets (Fig. 9), the phenyl rings of each PPh_2 unit are rendered non-equivalent. One set (coloured pale blue in Fig. 9) faces the non-coordinated pyridine ring, while the second set (green in Fig. 9) is directed towards the other side of the complex. The lowest energy dynamic process is the flipping of the diphenyl ether backbone of the POP ligand; with this motion persisting at 215 K, the four green Ph units are made equivalent, as are the four pale blue Ph rings.

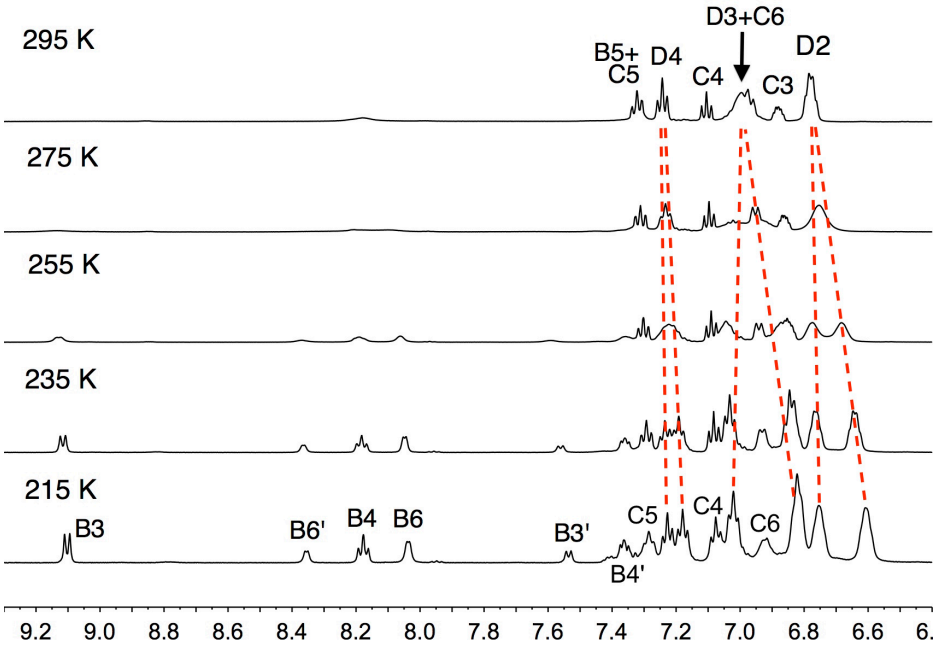

Fig. 7. Variable temperature 500 MHz ^{1}H NMR spectra of a CD_2Cl_2 solution of $[Cu_2(\mathbf{2})(POP)_2][PF_6]_2$. Chemical shifts in δ/ppm. See Scheme 2 for atom labelling.

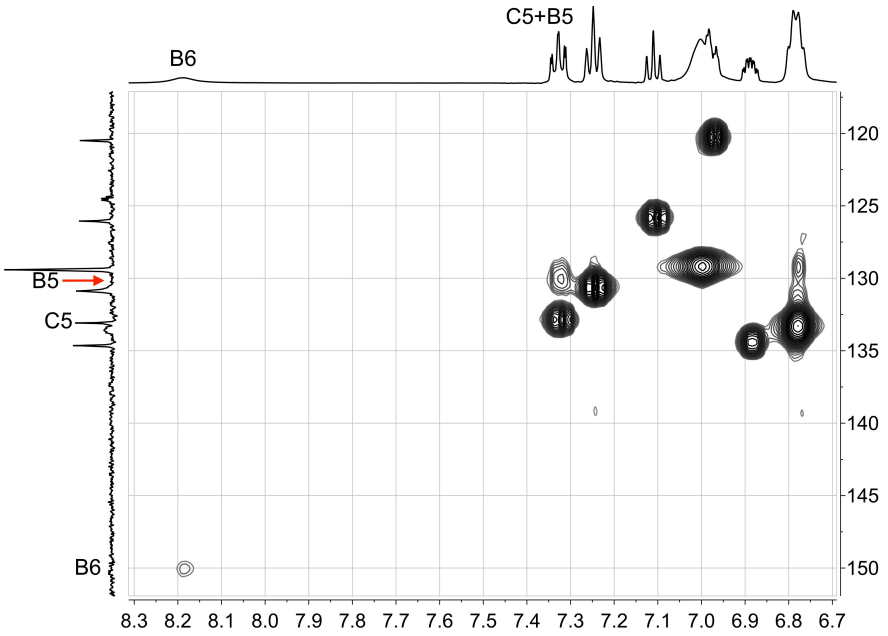

Fig. 8. Part of the HMQC spectrum (applied magnetic field = 11.75 T) of $[Cu_2(\mathbf{2})(POP)_2][PF_6]_2$ (in CD_2Cl_2 at 295 K) showing pyridine ring B6 and B5 signal assignments. The ^{13}C resonances are not resolved at 295 K in the 1D spectrum. Chemical shifts in δ/ppm.

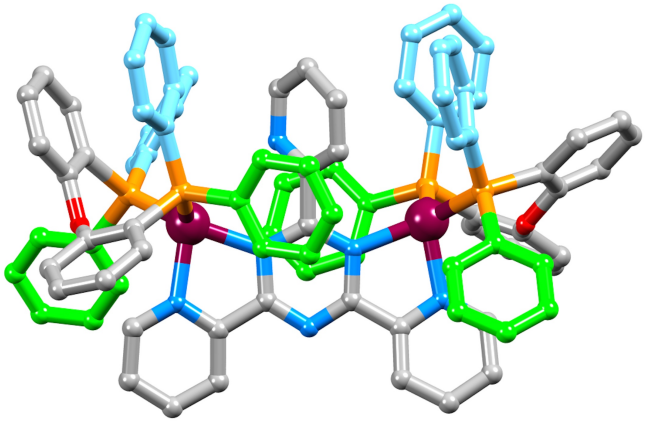

Fig. 9. Structure of the $[Cu_2(\mathbf{2})(POP)_2]^{2+}$ cation (from the crystallographically determined structure) with phenyl rings coloured to show the two sets observed in solution at 215 K. Colour online.

The room temperature solution ^{1}H NMR spectrum of $[Cu_2(\mathbf{2})(xantphos)_2][PF_6]_2$ consists largely of broad signals with the exception of sharp signals at δ 7.65 and 7.21 ppm (a doublet of doublets and a triplet, respectively). In addition to a septet assigned to the $[PF_6]^-$ ion, the $^{31}P\{^1H\}$ NMR spectrum exhibits a broadened singlet at δ –12.2 ppm consistent with one environment on the NMR timescale for the four PPh_2 groups. Across a series of related complexes, ^{13}C NMR chemical shifts tend to be diagnostic, and Fig. 10 compares parts of the ^{13}C NMR spectra of $[Cu_2(\mathbf{1})(xantphos)_2][PF_6]_2$ and $[Cu_2(\mathbf{2})(xantphos)_2][PF_6]_2$. Some similarities are clear, and combined with analysis of the HMQC spectrum (Fig. 11), it is possible to assign the signals for xantphos ring C protons and ^{13}C nuclei. Inspection of Fig. 10 and 11 indicates that there are two phenyl environments, analogous to the situation in $[Cu(Phbpy)(xantphos)][PF_6]$ at 295 K [36]. Variable temperature ^{1}H NMR spectra were recorded between 295 and 215 K and the aromatic regions of the spectra shown in Fig. 12 reveal that at least two dynamic processes are operative. The behaviour of the methyl signals for the xantphos CMe_2 unit is also consistent with this. The dynamic behaviour observed for $[Cu_2(\mathbf{2})(POP)_2][PF_6]_2$

(Fig. 7) coupled with the inversion of the two xanthene units in $[Cu_2(\mathbf{2})(xantphos)_2][PF_6]_2$ render the system complex and we have not investigated the processes in greater detail.

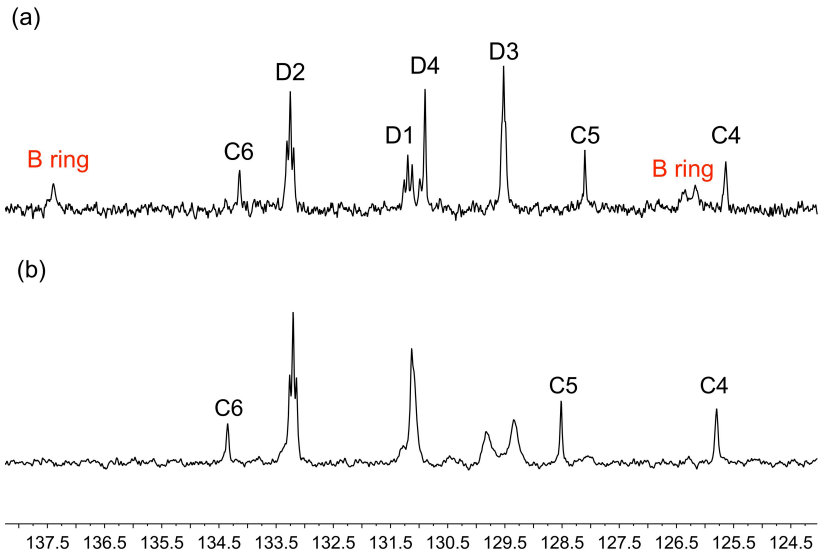

Fig. 10. Comparison of parts of the 126 MHz ^{13}C NMR spectra of CD_2Cl_2 solutions of (a) $[Cu_2(\mathbf{1})(xantphos)_2][PF_6]_2$ and (b) $[Cu_2(\mathbf{2})(xantphos)_2][PF_6]_2$. Chemical shifts in δ / ppm. See Scheme 2 for atom labelling.

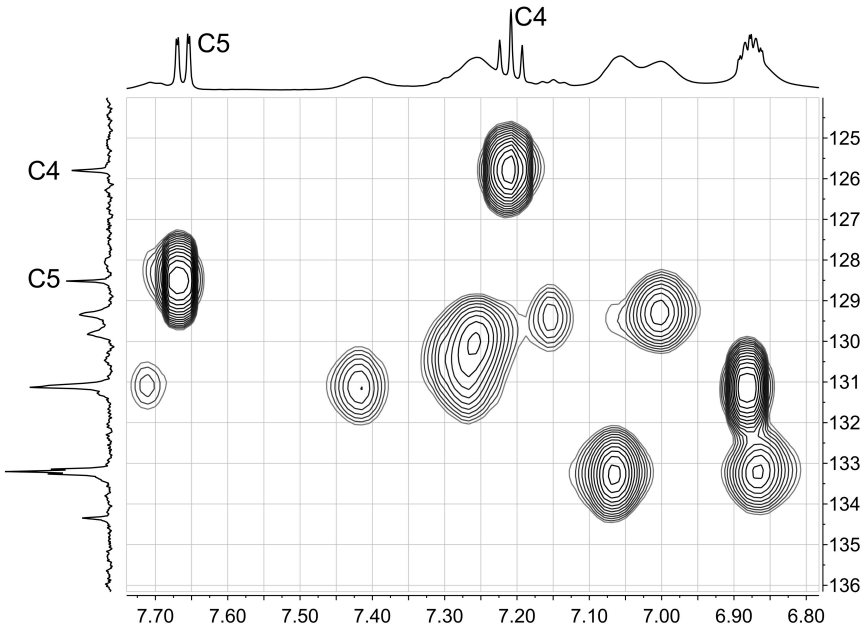

Fig. 11. Part of the HMQC spectrum (applied magnetic field = 11.75 T) of $[Cu_2(\mathbf{2})(xantphos)_2][PF_6]_2$. Chemical shifts in δ / ppm. See Scheme 2 for atom labelling.

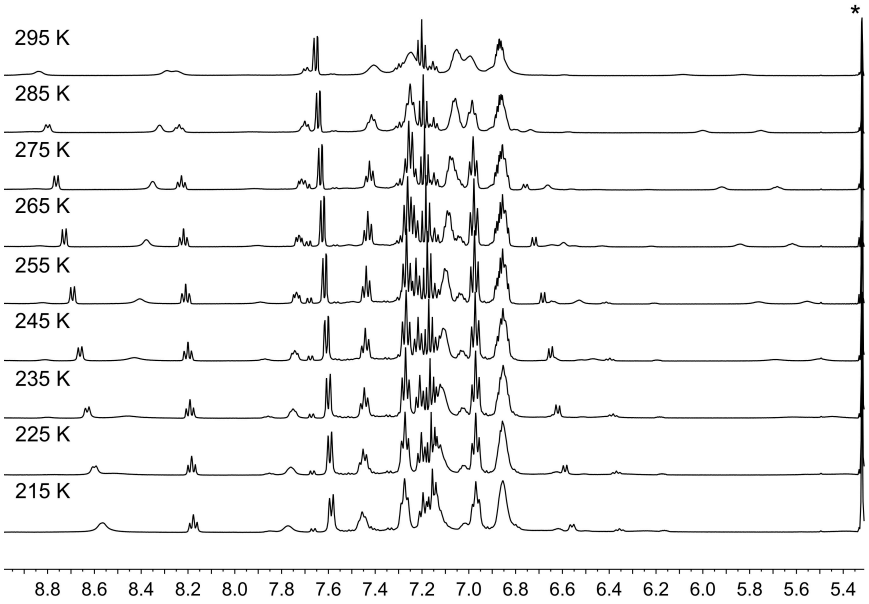

Fig. 12. Aromatic region of the variable temperature 500 MHz ^{1}H NMR spectra of a CD_2Cl_2 solution of $[Cu_2(\mathbf{2})(xantphos)_2][PF_6]_2$. Chemical shifts in *d* / ppm. * = residual $CHDCl_2$.

Photophysical properties

The solution absorption spectra of the $[Cu_2(N^N)(P^P)_2][PF_6]_2$ complexes are shown in Fig. 13. The high-energy bands are assigned to spin-allowed, ligand-based π*←π and π*←*n* transitions, and the profile of the spectrum below 380 nm depends upon the *N*-heterocycle ligand present in the complex. Each complex exhibits a broad band in the visible region, with λ_{max} = 485 nm for $[Cu_2(\mathbf{1})(POP)_2][PF_6]_2$ and $[Cu_2(\mathbf{1})(xantphos)_2][PF_6]_2$, and 487 or 489 nm for the complexes containing ligand **2**. This band is assigned to metal-to-ligand charge transfer (MLCT) and is red-shifted by up to 100 nm with respect to related mononuclear $[Cu(N^N)(P^P)][PF_6]$ complexes [5,6,10,14,36,37].

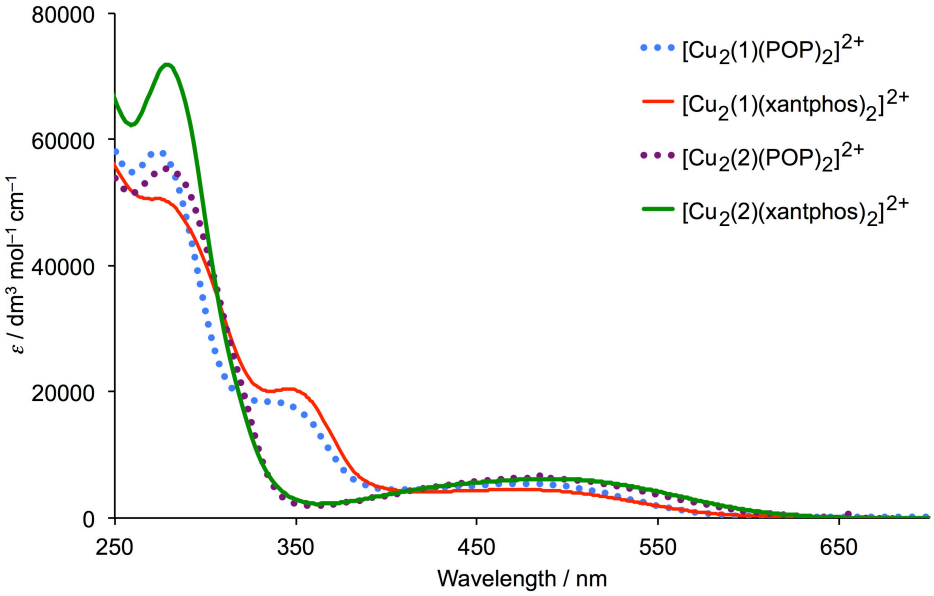

Fig. 13. Absorption spectra of $[Cu_2(N^N)(P^P)_2][PF_6]_2$ with N^N = **1** or **2**, and P^P = POP or xantphos (CH_2Cl_2, 2.5 x 10^{-5} mol dm^{-3}). Colour online.

At room temperature in both solution and the solid state, the complexes are very weakly emissive when excited at wavelengths between 270 and 490 nm, and we have not, therefore, investigated the emission behaviour in detail.

4. Conclusions

We have prepared and characterized the dinuclear copper(I) complexes $[Cu_2(\mathbf{1})(POP)_2][PF_6]_2$, $[Cu_2(\mathbf{2})(POP)_2][PF_6]_2$, $[Cu_2(\mathbf{1})(xantphos)_2][PF_6]_2$ and $[Cu_2(\mathbf{2})(xantphos)_2][PF_6]_2$. The bridging nature of **1** and **2** has been confirmed in the single crystal structures of $[Cu_2(\mathbf{1})(POP)_2][PF_6]_2$ and $[Cu_2(\mathbf{2})(POP)_2][PF_6]_2$. In the solid state, **1** and **2** both function as bis(bidentate) ligands with two and one non-coordinating pyridine ring, respectively. In solution at room temperature, each complex exhibits a single pyridine environment, consistent with dynamic behaviour. This has

been investigated in $[Cu_2(\mathbf{2})(POP)_2][PF_6]_2$ and $[Cu_2(\mathbf{2})(xantphos)_2][PF_6]_2$ by using variable temperature ^1H NMR spectroscopy. Cooling a solution of $[Cu_2(\mathbf{2})(POP)_2][PF_6]_2$ freezes out a process that renders the three pyridine rings equivalent; the lowest energy dynamic process is the flipping of the diphenyl ether backbone of the POP ligand. The dynamic processes in $[Cu_2(\mathbf{2})(xantphos)_2][PF_6]_2$ are more complex, with the inversion of the two xanthene units being coupled to the processes observed in $[Cu_2(\mathbf{2})(POP)_2][PF_6]_2$. The photophysical properties of the complexes have been investigated, but in contrast to the emissive properties exhibited by many [Cu(N^N)(P^P)][PF_6] complexes, $[Cu_2(\mathbf{1})(POP)_2][PF_6]_2$, $[Cu_2(\mathbf{1})(xantphos)_2][PF_6]_2$, $[Cu_2(\mathbf{2})(POP)_2][PF_6]_2$ and $[Cu_2(\mathbf{2})(xantphos)_2][PF_6]_2$ are only weakly emissive in solution or in the solid at room temperature.

Appendix 1 Supplementary data

Crystallographic data for all the complexes have been deposited with the CCDC (Cambridge Crystallographic Data Centre, 12 Union Road, Cambridge CB2 1EZ, UK; fax +44 1223 336 033; e-mail: deposit@ccdc.cam.ac.uk or www: http://www.ccdc.cam.ac.uk) and may be obtained free of charge on quoting the deposition numbers CCDC 1421984 and 1421985.

Acknowledgements

We thank the Swiss National Science Foundation (Grant numbers 200020_144500 and 200020_162631), the European Research Council (Advanced Grant 267816 LiLo) and the University of Basel for financial support. PD Daniel Häussinger, Y. Maximilian Klein and Thomas Müntener are thanked for assistance with the variable temperature NMR spectroscopic experiments.

References

1 R. D. Costa, E. Ortí, H. J. Bolink, F. Monti, G. Accorsi, N. Armaroli, Angew. Chem. Int. Ed. 51 (2012) 8178.

2 J. Emsley, The Elements, 3rd ed., Oxford University Press, 1998.

3 See for example: C. E. Housecroft, E. C. Constable, Chem. Soc. Rev. 44 (2015) 8386.

4 F. Dumur, Org. Electronics 21 (2015) 27.

5 R. D. Costa, D. Tordera, E. Ortí, H. J. Bolink, J. Schönle, S. Graber, C. E. Housecroft, E. C. Constable, J. A. Zampese, J. Mater. Chem. 21 (2011) 16108.

6 S. Keller, E. C. Constable, C. E. Housecroft, M. Neuburger, A. Prescimone, G. Longo, A. Pertegás, M. Sessolo, H. J. Bolink, Dalton Trans. 43 (2014) 16593.

7 A. Kaeser, O. Moudam, G. Accorsi, I. Séguy, J. Navarro, A. Belbakra, C. Duhayon, N. Armaroli, B. Delavaux-Nicot, J.-F. Nierengarten, Eur. J. Inorg. Chem. (2014) 1345.

8 N. Armaroli, G. Accorsi, M. Holler, O. Moudam, J. F. Nierengarten, Z. Zhou, R. T. Wegh, R. Welter, Adv. Mater. 18 (2006) 1313.

9 R. Czerwieniec, H. Yersin, Inorg. Chem. 54 (2015) 4322.

10 K. Zhang, D. Zhang, Spectrochim. Acta A 124 (2013) 341.

11 L. Bergmann, J. Friedrichs, M. Mydlak, T. Baumann, M. Nieger, S. Bräse, Chem. Commun. 49 (2013), 6501.

12 E. Mejía, S.-P. Luo, M. Karnahl, A. Friedrich, S. Tschierlei, A.-E. Surkus, H. Junge, S. Gladiali, S. Lochbrunner, M. Beller, Chem. Eur. J. 19 (2013) 15972.

13 X.-L. Chen, R. Yu, Q.-K. Zhang, L.-J. Zhou, X.-Y. Wu, Q. Zhang, C.-Z. Lu, Chem. Mater. 25 (2013) 3910.

14 I. Andrés-Tomé, J. Fyson, F. Baiao Dias, A. P. Monkman, G. Iacobellis, P. Coppo, Dalton Trans. 41 (2012), 8669.

15 C. L. Linfoot, M. J. Leitl, P. Richardson, A. F. Rausch, O. Chepelin, F. J. White, H. Yersin, N. Robertson, Inorg. Chem. 53 (2014) 10854.

16 S.-M. Kuang, D. G. Cuttell, D. R. McMillin, P. E. Fanwick, R. A. Walton, Inorg. Chem. 41 (2002) 3313.

17 T. Tsubomura, K. Kimura, M. Nishikawa, T. Tsukuda, Dalton Trans. 44 (2015) 7554.

18 A. Kaeser, M. Mohankumar, J. Mohanraj, F. Monti, M. Holler, J.-J. Cid, O. Moudam, I. Nierengarten, L. Karmazin-Brelot, C. Duhayon, B. Delavaux-Nicot, N. Armaroli, J.-F. Nierengarten, Inorg. Chem. 52 (2013) 12140.

19 C. Femoni, S. Muzzioli, A. Palazzi, S. Stagni, S. Zacchini, F. Monti, G. Accorsi, M. Bolognesi, N. Armaroli, M. Massi, G. Valenti, M. Marcaccio, Dalton Trans. 42 (2013) 997.

20 X.-Y. Feng, X.-L. Xin, Y.-M. Guo, L.-L. Chen, Y.-Y. Liang, M. Xun X.-L. Li, Polyhedron 101 (2015) 23.

21 M. J. Leitl, F-R. Küchle, H. A. Mayer, L. Wesemann, H. Yersin, J. Phys. Chem. A 117 (2013) 11823.

22 J.-L. Chen , W. Gu , X.-F. Cao , H.-R. Wen, R. Hong , J. Coord. Chem. 64 (2011) 1903.

23 B. Gil, G. A. Cooke, D. Nolan, G. M. Ó. Máille, S. Varughese, L. Wang, S. M. Draper, Dalton Trans. 40 (2011) 8320.

24 T. Tsubomura, S. Enoto, S. Endo, T. Tamane, K. Matsumoto, T. Tsukuda, Inorg. Chem. 44 (2005) 6373.

25 C. Bizzarri, C. Strabler, J. Prock, B. Trettenbrein, M. Ruggenthaler, C.-H. Yang, F. Polo, A. Iordache, P. Brüggeller, L. De Cola, Inorg. Chem. 53 (2014) 10944.

26 J.-J. Cid, J. Mohanraj, M. Mohankumar, M. Holler, F. Monti, G. Accorsi, L. Karmazin-Brelot, I. Nierengarten, J. M. Malicka, M. Cocchi, B. Delavaux-Nicot, N. Armaroli, J.-F. Nierengarten, Polyhedron 82 (2014) 158.

27 D. Volz, M. Wallesch, S. L. Grage, J. Göttlicher, R. Steininger, D. Batchelor, T. Vitova, A. S. Ulrich, C. Heske, L. Weinhardt, T. Baumann and S. Bräse, Inorg. Chem. 53 (2014) 7837.

28 N. S. Murray, S. Keller, E. C. Constable, C. E. Housecroft, M. Neuburger, A. Prescimone, Dalton Trans. 44 (2015) 7626.

29 Bruker Analytical X-ray Systems, Inc., 2006, APEX2, version 2 User Manual, M86-E01078, Madison, WI.

30 P. W. Betteridge, J. R. Carruthers, R. I. Cooper, K. Prout, D. J. Watkin, J. Appl. Cryst. 36 (2003) 1487.

31 I. J. Bruno, J. C. Cole, P. R. Edgington, M. K. Kessler, C. F. Macrae, P. McCabe, J. Pearson, R. Taylor, Acta Crystallogr., Sect. B 58 (2002) 389.

32 C. F. Macrae, I. J. Bruno, J. A. Chisholm, P. R. Edgington, P. McCabe, E. Pidcock, L. Rodriguez-Monge, R. Taylor, J. van de Streek, P. A. Wood, J. Appl. Cryst.41 (2008) 466.

33 A. L. Spek, Acta Crystallogr., Sect. D 65 (2009) 148.

34 O. Moudam, A. C. Tsipis, S. Kommanaboyina, P. N. Horton, S. J. Coles, RSC Adv. 5 (2015) 95047.

35 Y.-P. Wang, X.-H. Hu, Y.-F. Wang, J. Pan, X.-Y. Yi, Polyhedron 102 (2015) 782.

36 S. Keller, A. Pertegás, G. Longo, L. Martinez, J. Cerdá, J.M. Junquera-Hernández, A. Prescimone, E. C. Constable, C. E. Housecroft, E. Ortí and H. J. Bolink, *J. Mater. Chem. C*, manuscript in revision TC-ART-11-2015-003725.

37 S. Xu, J. Wang, F. Zhao, H. Xia and Y. Yang, J. Mol. Model. 21 (2015) 1.